Chemistry–A European Journal

Full Paper
doi.org/10.1002/chem.202101247

Chemistry
Europe
European Chemical
Societies Publishing

Thermally Activated Delayed Fluorescence and Phosphorescence Quenching in Iminophosphonamide Copper and Zinc Complexes

Bhupendra Goswami[++],[a] Thomas J. Feuerstein[++],[a] Ravi Yadav,[a] Sergei Lebedkin,[b] Pit J. Boden,[c] Sophie T. Steiger,[c] Gereon Niedner-Schatteburg,[c] Markus Gerhards[+],[c] Manfred M. Kappes,[b, d] and Peter W. Roesky*[a]

Abstract: The synthesis of copper and zinc complexes of four variably substituted iminophosphonamide ligands is presented. While the copper complexes form ligand-bridged dimers, the zinc compounds are monomeric. Due to different steric demand of the ligand the arrangement of the ligands within the dimeric complexes varies. Similar to the structurally related iminophosphonamide complexes of alkali metals and calcium, the steady-state and time-resolved photoluminescence (PL) of four of the seven compounds studied here as solids in a temperature range of 5–295 K can be described within the scheme of thermally activated delayed fluorescence (TADF). Accordingly, they exhibit bright blue-green phosphorescence at low temperatures (<100 K), which turns into delayed fluorescence by increasing the temper-ature. However, unusually, the fluorescence is practically absent in two copper complexes which otherwise still conform to the TADF scheme. In these cases, the excited singlet states decay essentially non-radiatively and their thermal population from the corresponding low-lying triplet states efficiently quenches PL (phosphorescence). Three other copper and zinc complexes only exhibit prompt fluorescence, evidencing a wide variation of photophysical properties in this class of compounds. The excited states of the copper complex with especially pronounced phosphorescence quenching were also investigated by low-temperature time-resolved infrared spectroscopy and quantum chemical calculations.

Introduction

The term imino-aza-phosphorus(V)-ligand covers a wide variety of ligands containing both nitrogen and phosphorus atoms. The common feature of these ligands is the presence of one or more terminal R–N=P units.[1] Amongst this class are the monoanionic diiminophosphinates of the general formula [R$_2$P-(NR')$_2$]$^-$, which are alternatively termed iminophosphonamides. In analogy to amidinates which are often compared with carboxylates, they can be regarded as the nitrogen analogues of phosphinate anions [R$_2$PO$_2$]$^-$.[2] Like amidinates, iminophosphonamides are chelating ligands, forming four-membered metallacycles upon metal coordination. Therefore, these compounds also belong to a general class of NXN donor ligands. Among these ligands, iminophosphonamides deserve special interest due to several features: (i) Due to the zwitterionic nature of the R$_2$P$^+$(NR'$^-$)$_2$ (NPN) ligand the σ-donor properties of the nitrogen atoms are enhanced.[3] For instance, recently, Nakata et al. found both experimentally and theoretically that iminophosphonamide-chlorosilylene is a stronger σ-donor in comparison with the common non-heterocyclic carbenes (NHCs) and silylenes (NHSis).[4] (ii) Due to a rather long P–N bond of *approx.* 1.60 Å iminophosphonamides exhibit a wider bite angle than amidinates or, more generally, other NXN

[a] Dr. B. Goswami,[++] Dr. T. J. Feuerstein,[++] Dr. R. Yadav, Prof. Dr. P. W. Roesky
Institute of Inorganic Chemistry
Karlsruhe Institute of Technology (KIT)
Engesserstrasse 15, 76131 Karlsruhe (Germany)
E-mail: roesky@kit.edu

[b] Dr. S. Lebedkin, Prof. Dr. M. M. Kappes
Institute of Nanotechnology
Karlsruhe Institute of Technology (KIT)
Hermann-von-Helmholtz-Platz 1, 76344 Eggenstein-Leopoldshafen (Germany)

[c] P. J. Boden, S. T. Steiger, Prof. Dr. G. Niedner-Schatteburg, Prof. Dr. M. Gerhards[+]
Fachbereich Chemie und Forschungszentrum OPTIMAS
TU Kaiserslautern
67663 Kaiserslautern (Germany)

[d] Prof. Dr. M. M. Kappes
Institute of Physical Chemistry
Karlsruhe Institute of Technology (KIT)
Fritz-Haber Weg 2, 76131 Karlsruhe (Germany)

[++] These authors contributed equally to this work.

[+] Deceased December 28, 2020.

🖥 Supporting information for this article is available on the WWW under https://doi.org/10.1002/chem.202101247

This manuscript is part of a Special Issue "Cooperative effects in hetero-metallic complexes".

Chemistry–A European Journal

Full Paper
doi.org/10.1002/chem.202101247

Chemistry Europe
European Chemical
Societies Publishing

bidentate chelating ligands like boraamidinates (X=BR),[5] triazenides (X=N)[6] and sulfinamidinates (X=SR).[7,8] (iii) Besides the σ-donor strength, the high steric demand of the pentavalent phosphorous atom further contributes to the stabilization of metal centers. (iv) Finally, yet importantly, a ^{31}P nucleus in the ligand backbone may beneficially serve as a spectroscopic marker for monitoring chemical transformations.[9]

Moreover, metal complexes of iminophosphonamides are attractive from the photophysical point of view. Indeed, metal coordination of ligands containing both phosphorous and nitrogen sites has frequently resulted in compounds demonstrating interesting photoluminescence (PL) properties.[10] This holds true also for iminophosphonamides. Recently, we reported on the alkali metal complexes of a chiral iminophosphonamine ligand.[11] In the solid state, in contrast to the fluorescent ligand, these complexes show efficient blue-green long-lived phosphorescence at low temperatures (<100 K) and thermally activated delayed fluorescence (TADF)[12] above ≈150 K with quantum yields of up to 36% at room temperature. This surprising difference has been attributed to the dimeric ligand arrangement in the alkali metal complexes, enabling symmetry-breaking intramolecular charge transfer between the 'monomeric' ligand units, which can strongly enhance intersystem crossing (ISC) and triplet formation.[13]

The TADF is then facilitated by a small energy gap (≈400–700 cm^{-1}) between the relaxed excited singlet (S_1) and first triplet (T_1) states of the iminophosphonamine ligand and its complexes. This results in thermal population of the S_1 state from the lower-lying triplet state and in S_1 fluorescence dominating at elevated temperatures. Similar observations were made for the related calcium complexes.[14]

These findings encouraged us to investigate coordination of the iminophosphonamine ligands with other metals, including transition metals. Herein we report on the synthesis of copper(I) and zinc(II) iminophosphonamide complexes. Copper(I) complexes are generally characterized by a large impact of the metal centers on the PL properties as well as a high number of

reported TADF emitting compounds.[15] Copper(I) complexes of NXN ligands are known to adopt dinuclear forms with two closely arranged metal centers, which may result in metallophilic interactions.[16] Additionally, linear structures are usually observed with parallel-aligned ligands. In contrast, zinc(II)-NXN complexes, due to a central tetrahedral coordination sphere, generally form monometallic structures with orthogonally arranged ligands.

Depending on the metal and ligand substituents, a very different PL behavior was observed for the copper(I) and zinc(II) iminophosphonamide complexes studied as solids in a temperature interval of 5–295 K, ranging from prompt fluorescence to TADF and long-lived phosphorescence. We moreover utilized step-scan FTIR analysis to characterize the excited triplet state of a selected copper complex and its dynamics on the microsecond time scale. The spectroscopic experiments were supported by density functional theory (DFT) modelling.

Results and Discussion

At first the synthesis was focused on copper(I) complexes of the four differently substituted, previously described iminophosphonamide ligands. As a starting point the lithiated ligand [Li$_2${(R)-PEPIA}$_2$] ((R)-PEPIA=P,P-diphenyl-N,N'-bis((R)-1-phenylethyl)phosphinimidic amide) was reacted with copper(I) chloride in a metathesis reaction to yield the dinuclear copper(I) complex [Cu$_2${(R)-PEPIA}$_2$] (**1**) (Scheme 1). The ^{1}H NMR spectrum of **1** is quite similar to that of the lithiated ligand. The most pronounced difference is the $^3J_{PH}$ constant for the coupling between the ^{i}Pr-CH protons and the phosphorous atom, which amounts to $^3J_{PH}$=18.8 Hz for **1** and $^3J_{PH}$=21.6 Hz for [Li$_2${(R)-PEPIA}$_2$]. The ^{13}C{^{1}H} NMR spectrum is comparable to the spectrum of the parent compound as well. However, a notably larger chemical shift of δ=39.6 ppm is observed in the ^{31}P{^{1}H} NMR spectrum of **1** (δ=20.6 ppm for [Li$_2${(R)-PEPIA}$_2$]). Furthermore, whereas a *pseudo*-quartet resonance due to $^2J_{PLi}$ coupling
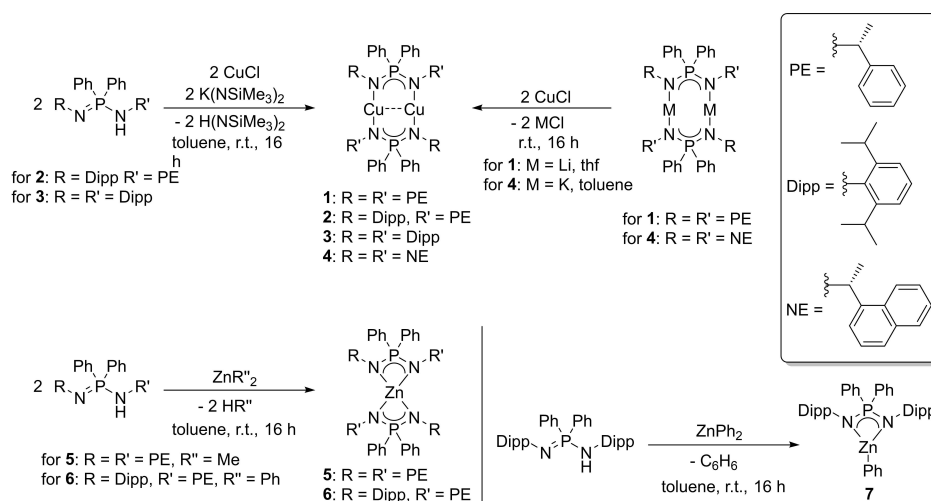
Scheme 1. Synthesis of compounds **1–7**.

Chemistry–A European Journal

Full Paper
doi.org/10.1002/chem.202101247

Chemistry Europe
European Chemical
Societies Publishing

is observed for the lithium complex, a singlet resonance is detected for the copper compound **1** (Figure S3.3). In the IR spectrum of **1** (Figure S4.1) the lack of any vibration modes above 3054 cm^{-1} indicates the absence of N–H groups. Single crystals suitable for X-ray crystallography were grown by recrystallization from *n*-hexane, whereby complex **1** crystallizes in the chiral orthorhombic space group $P2_12_12_1$. As expected, the molecular structure of compound **1** in the solid state represents a dinuclear molecule in which two copper(I) ions, in close contact, bridge two ligands. The Cu1···Cu2 distance of 2.534(2) Å is in the usual range for cuprophilic interactions.[17] The NPN angles (N1-P1-N2 110.1(5)° and N4-P2-N3 110.3(5)°) are slightly widened in comparison with the X-ray data for the starting compound (N1-P1-N2 108.52(14)° and N3-P2-N4 99.7(2)° in [Li$_2${(*R*)-PEPIA}$_2$]). Moreover, the N1-P1-P2-N3 torsion angle between the two ligands of 140.223(2)° in **1** is not far from 180°, which is ascribed to the affinity of copper(I) ions for the linear coordination geometry as well as to the reduction of steric restrains between the nitrogen substituents. Accordingly, the phenyl moieties on the nitrogen atoms N1 and N3 protrude below the paper plane in Figure 1, while the respective moieties on N2 and N4 emerge from it.

Next, we moved on to the synthesis of the Cu(I) complex of the bulkier asymmetric ligand (*R*)-HPE^{Dipp}PIA ((*R*)HPE^{Dipp}PIA = *P,P*-diphenyl-*N*-((*R*)-1-phenylethyl),*N*′-(2′,6′-diisopropylaniline)-phosphinimidic amide). The protonated ligand was straightforwardly reacted in a one-pot synthesis with equivalent amounts of potassium bis(trimethylsilyl)amide (KHMDS) and CuCl. After workup [Cu$_2${(*R*)-PE^{Dipp}PIA}$_2$] (**2**) was obtained as a white crystalline solid. All resonances in the ^{1}H and ^{13}C{^{1}H} NMR spectra (Figures S3.4 and S3.5) can be assigned to the respective Dipp and PE substituents as well as to the aromatic protons. Furthermore, a similar chemical shift of the singlet resonance in the ^{31}P{^{1}H} NMR ($\delta = 38.0$ ppm) is observed for complex **2** in comparison to **1**.

This signal is significantly shifted downfield as compared to the phosphorous resonance at $\delta = -10.9$ ppm for (*R*)-HPE^{Dipp}PIA. Single crystals of **2** were obtained after recrystallization from hot toluene. The compound crystallizes in the tetragonal chiral space group $P4_32_12$. The molecular structure shows that two copper centers are bridged by the iminophosphonamide

ligands, in a structure similar to that of **1** and the related structure [{Ph$_2$P(NSiMe$_3$)$_2$}$_2$Cu$_2$].[16a] The two flanking Dipp groups in complex **2** are trans positioned, probably to minimize the steric repulsion. The NPN angles (N1-P1-N2 109.5(2)°) in the molecular structure of complex **2** (Figure 1) are nearly identical to the NPN angles for **1**. However, the ligands in **2** are aligned nearly coplanar with a N1-P1-P2-N4 torsion angle of 179.66(2)°. This is attributed to the higher steric demand of the two Dipp substituents. The Cu-N bond lengths are almost identical and lie in the range of previously reported complexes. The Cu1···Cu2 distance of 2.5324(7) Å is nearly the same as observed for **1**.

The next step in the systematic study of the influence of the ligand steric demand on the structure and photophysical properties of the copper(I) complexes was the synthesis of complex **3** with four Dipp substituents incorporating the achiral symmetric ligand *P,P*-diphenyl-*N,N*′-bis(2,6-diisopropylphenyl)phosphinimidic amine (H-DippPIA).[9] The desired product [Cu$_2${DippPIA}$_2$] (**3**) was obtained by a similar one-pot procedure as described for **2** (Scheme 1) in form of colorless crystals. In the ^{1}H NMR and ^{13}C{^{1}H} NMR spectra of **3** all signals can be ascribed to the Dipp substituted iminophosphonamide ligand. The multiplicity is also in full agreement with the deprotonated symmetrically substituted ligand. However, the singlet resonance in the ^{31}P{^{1}H} NMR spectrum of **3** ($\delta = 8.4$ ppm) is significantly shifted to lower ppm in comparison with **1** and **2**. Complex **3** crystallizes in the monoclinic space group $P2_1/n$ with half of a molecule in the asymmetric unit. Like complex **2**, compound **3** has an inversion center in the middle of the molecule. The structural features of **3** are almost similar to those observed for **1** and **2**. The intermetallic Cu1···Cu1′ interaction in **3** is 2.5292(10) Å, which is consistent with that observed in the related compounds [{(2,6-Me$_2$C$_6$H$_3$N)$_2$C(H)}$_2$Cu$_2$][18] and [{^{i}PrNC(Me)N^{i}Pr}$_2$Cu$_2$].[19] The N1-Cu1-N2′ bond angle amounts to 176.82(12)° which is close to linearity and in consistence with the arrangements in complexes **1** and **2**. The respective Cu1-N1 and Cu1′-N2 bond lengths of 1.895(3) and 1.886(3) Å in **3** are slightly longer than those observed for [{(2,6-Me$_2$C$_6$H$_3$N)$_2$C-(H)}$_2$Cu$_2$] (1.869(1) Å). Furthermore, the N1-P1-P1′-N1′ torsion angle of 180.00(2)° in **3** is the highest of compounds **1**-**3**, presumably because of the higher steric demand induced by the Dipp-groups.
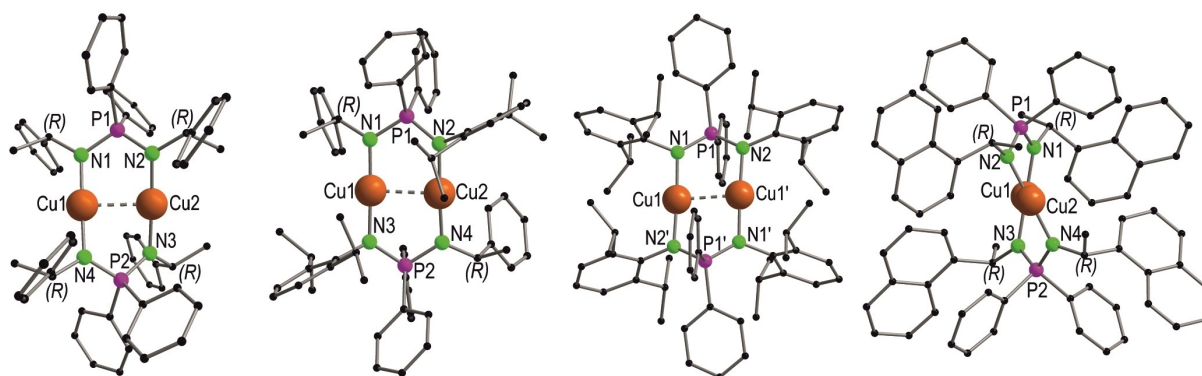
Figure 1. Molecular structure of compounds **1**–**4** (from left to right) in the solid state. Structural parameters are given in the supporting information.

Chemistry–A European Journal

Full Paper
doi.org/10.1002/chem.202101247

Chemistry Europe
European Chemical
Societies Publishing

After the successful isolation of the binuclear copper complexes **1-3**, the substituent groups were altered to increase the π-character of the ligand. It is well known that, functionalized extended π-conjugated systems may strongly influence photophysical properties, for example due to intermolecular π-π interactions.[20] In this regard, the [(R)-NEPIA]⁻ ligand ((R)-NEPIA = P,P-diphenyl-N,N'-bis((R)-1-naphthylethyl)phosphinimidic amide) was prepared, featuring naphthyl groups at the nitrogen centers. [Cu₂{(R)-NEPIA}₂] (**4**) was obtained from the salt metathesis reaction of CuCl and the potassium salt of [(R)-NEPIA]⁻ (Scheme 1). After extraction and standard workup procedure, it was isolated as a colorless solid. The ¹H NMR spectrum of complex **4** (Figure S3.10) is consistent with a symmetric arrangement in solution. More precisely, the characteristic doublet of quartets at $\delta = 5.12$ ($^3J_{PH} = 16.3$ Hz, $^3J_{HH} = 6.4$ Hz) is assigned to the naph(CH)CH₃ protons, whereas the doublet at $\delta = 1.9$ ppm ($^3J_{HH} = 6.5$ Hz) is attributed to the naph(CH)CH₃ protons. In the ¹³C{¹H} NMR spectrum (Figure S3.11), the methine and methyl moieties can be assigned to the resonances at $\delta = 50.6$ ppm (naph(CH)CH₃) and $\delta = 31.3$ ppm (naph(CH)CH₃), respectively.

The purity of the complex can be assessed by the detection of a single resonance at $\delta = 40.2$ ppm in the ³¹P{¹H} NMR spectrum, which is significantly shifted upfield as compared to $\delta = 38.0$ ppm in the dicopper(I) complex **2**. Complex **4** crystallizes in the orthorhombic chiral space group $P2_12_12_1$ with one molecule in the asymmetric unit. The Cu1···Cu2 distance in complex **4** amounts 2.5054(8) Å, which is within the typical range of cuprophilic interactions.[17] The N1-Cu1-N4 (175.6(2)°) and N2-Cu2-N3 (174.7(2)°) bond angles are close to linearity. Furthermore, the P-N contact lengths in **4** are almost equal (P1-N1 1.611(4), P1-N2 1.608(4), P2-N3 1.611(4) and P2-N4 1.612(4)), suggesting delocalization of the anionic charge over the NPN backbone.

Next, we focused on the synthesis of zinc(II) complexes. As a starting point, two equivalents of the protonated iminophosphonamide (R)-HPEPIA were reacted in a base elimination reaction with dimethyl zinc to yield the Zn(II) complex [Zn{(R)-PEPIA}₂] (**5**) (Scheme 1). The ¹H and ¹³C{¹H} NMR spectra of **5** (Figures S3.13 and S3.14) appear quite similar to the corresponding spectra for the Cu(I) complex **1**. In consistency in the ³¹P{¹H} NMR spectrum a single resonance is

observed at $\delta = 35.7$ ppm which is located in a comparable range as for **1–4**. Furthermore, the complex can be clearly detected via EI mass spectrometry as a molecular peak [M⁺] at $m/z = 910.3507$ (Figure S5.2). Single crystals of compound **5** were obtained from *n*-pentane. The complex crystallizes in the triclinic space group $P1$ with two molecules in the asymmetric unit. The Zn–N bond lengths are all in a narrow range of 2.025(3)–2.054(3) Å. Besides the iminophosphonamide bite angles (N1-Zn-N2 74.34(12)° and N3-Zn1-N4 74.48(12)°), all N-Zn-N angles are in the range of 128.19(13)–130.83(13)°. Therefore, the Zn(II) core is coordinated distorted tetrahedrally by the four nitrogen atoms, which is in agreement with the calculated distortion parameters with the program SHAPE 2.1 (Table S6.2).[21] Furthermore, the two ligands are aligned nearly perfectly opposite towards each other, with a nearly rectangular torsion angle of N1-P1-P2-N3 of 92.92(2)° (Figure 2).

Furthermore, in order to vary the ligand in the coordination sphere of a Zn(II) complex, the (R)-HPE^{Dipp}PIA ligand was reacted with ZnPh₂ in a molar ratio of 2:1 (Scheme 1), which resulted in the formation of the homoleptic zinc complex [Zn{(R)-PE^{Dipp}PIA}₂] (**6**). The disappearance of the NH resonance in the ¹H NMR spectrum indicated the successful formation of complex **6**. Furthermore, the ¹H NMR spectrum of **6** exhibits a single set of resonances suggesting a certain degree of symmetry in solution. The Ph(CH)CH₃ signal appears as a doublet of quartets in the aliphatic region at $\delta = 3.79$ ppm ($^3J_{PH} = 18.57$, $^3J_{HH} = 6.53$ Hz). A doublet at $\delta = 1.37$ ppm ($^3J_{HH} = 6.52$ Hz) is assigned to the Ph(CH)CH₃ protons. The purity of complex **6** was further confirmed by the detection of only one peak at $\delta = 37.5$ ppm in the ³¹P{¹H} NMR spectrum, which is significantly shifted downfield compared to $\delta = -10.9$ ppm for (R)-HPE^{Dipp}PIA. Complex **6** crystallizes in the orthorhombic space group $P2_12_12_1$ with one molecule in the asymmetric unit. The central zinc atom is coordinated by four nitrogen atoms of two [(R)-PE^{Dipp}PIA]⁻ ligands. However, in contrast to compound **5** the central zinc atom is closer to a square planar coordination geometry with nearly parallelly aligned NPN backbones, as indicated by the calculated distortion parameters (Figure S6.8 and Table S6.2). In order to minimize the steric repulsion, the Dipp groups adopt *trans* positions with respect to the central metal core. Furthermore, due to the unsymmetrical nature of the ligand the Zn–N bonds are not identical and are in the
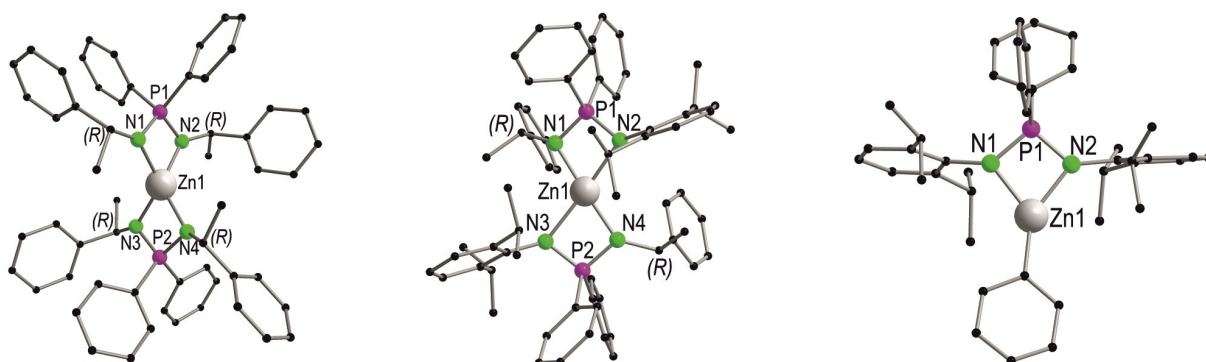
Figure 2. Molecular structure of compounds **5**, **6** and **7** (from left to right) in the solid state. Structural parameters are given in the supporting information.

Chemistry–A European Journal

Full Paper
doi.org/10.1002/chem.202101247

Chemistry
Europe
European Chemical
Societies Publishing

range of 1.994(3)–2.197(3) Å. The bite angles of the iminophosphonamides in complex **6** (N1-Zn-N2 72.06(11)° and N3-Zn-N4 71.94(10)°) are slightly narrower than the corresponding bite angles in **5**.

In order to synthesize a zinc analogue of complex **3**, ZnPh$_2$ was reacted with HDippPIA in a 1:2 molar ratio. However, formation of the heteroleptic complex [{DippPIA}ZnPh] (**7**) was observed in contrast to the homoleptic complexes **5** and **6**. This might be due to the sterically hindered nature of HDippPIA which prevents the coordination of two ligands on the same Zn(II) metal center. Complex **7** could be reproduced with a 1:1 molar ratio of the reagents (Scheme 1) and exhibits good solubility in common organic solvents such as thf, diethylether and toluene and is even slightly soluble in *n*-pentane. The heteroleptic nature of complex **7** was confirmed by ^{1}H NMR spectroscopy and no signs of ligand redistribution to a homoleptic complex were observed. The aromatic resonances appear in the range of $\delta = 7.63$–6.77 ppm. The characteristic septet of the C*H*(CH$_3$)$_2$ moiety appears at $\delta = 3.88$ ppm ($^3J_{HH} = 6.81$ Hz), whereas the CH(C*H*$_3$)$_2$ resonance appears as doublet at $\delta = 1.03$ ppm ($^3J_{PH} = 6.87$ Hz). In the ^{13}C{^{1}H} NMR spectrum, the resonances at $\delta = 29.4$ ppm and $\delta = 24.1$ ppm can be attributed to *C*H(CH$_3$)$_2$ and CH(*C*H$_3$)$_2$, respectively. In the ^{31}P{^{1}H} NMR spectrum, the appearance of a single peak at $\delta = 17.2$ ppm further indicates the purity of the product. The molecular structure of **7** is similar to that of the related [{DippPIA}ZnMe] and [{DippPIA}ZnEt] complexes reported by Stasch.[9]

The Zn-N (Zn-N1 2.027(2) Å and Zn-N2 1.996(2) Å) and Zn-C (Zn-C37 1.931(3) Å) bond lengths in **7** are consistent with those in related complexes. The N1-Zn-N2 acute bite angle of 74.50(8)° in complex **7** is wider than that of 65.9(2)° in the related amidinate complex [{MeC(NDipp)$_2$}$_2$Zn].

Photoluminescence properties

The structures and dimeric ligand arrangements of the bimetallic copper complexes **2**, **3** and especially **1** are close to those of the previously reported iminophosphonamide alkali metal complexes [M$_2${(*R*)-PEPIA}$_2$] (M = Li, Na, K, Rb and Cs, see Scheme 1).[11] The monometallic zinc complexes **5** and **6** coordinating two iminophosphonamide ligands are analogous to the calcium complexes [Ca{(*R*)-PEPIA}$_2$].[14] In view of the bright phosphorescence and thermally activated delayed fluorescence (TADF) observed for the alkali metal and calcium derivatives,[11,14] a comparison with PL properties of the copper and zinc complexes **1–7** appears particularly interesting. Figures 3 and 4 show PL excitation (PLE) and emission spectra of the solid (polycrystalline) samples of **1–4** and **5–7**, respectively, at selected temperatures between 5 and 295 K, together with the emission intensity as a function of temperature. The spectra at further intermediate temperatures are presented in Figures S7.1-7 in the supporting information. Below T ≈ 50 K all complexes intensely emit at 450–530 nm under UV photoexcitation. The onset of absorption (PLE) at 360–400 nm (shifted to ca. 330 and 450 nm in **7** and **6**, respectively) is consistent with the white to pale yellow appearance of the powder
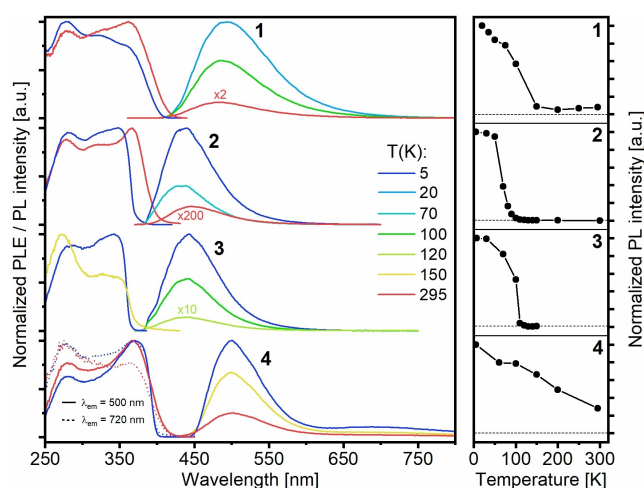
Figure 3. Left: Normalized photoluminescence excitation (PLE) and emission (PL) spectra of the solid bimetallic copper compounds **1–4** at temperatures between 5 and 295 K. The PL/ PLE spectra were excited at 350 (**1**), 340 (**2**), 340 (**3**) and 350 nm (**4**) and recorded at 480 (**1**), 450 (**2**), 460 (**3**) and 500 nm (**4**), if not indicated otherwise. Right: Integral PL intensities versus temperature in the range of 5–295 K (also shown on the logarithmic scale for **2** and **3** in Figures S7.2 and S7.3).
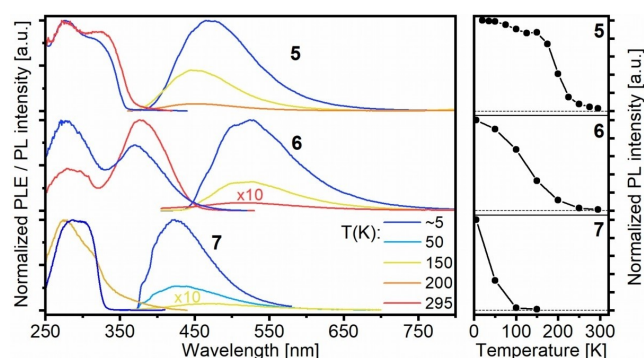
Figure 4. Left: Normalized photoluminescence excitation (PLE) and emission (PL) spectra of the solid monometallic zinc complexes **5–7** at temperatures between 5 and 295 K. The PL/ PLE spectra were excited at 330 (**5**), 380 (**6**), and 300 nm (**7**) and recorded at 480 (**5**), 520 (**6**) and 450 nm (**7**). Right: Integral PL intensities versus temperature in the range of 5–295 K.

samples. Similar spectra were observed for the alkali metal and calcium complexes, indicating related structures.[11,14] The low-temperature emission of the latter and dimeric complexes **1–3** and **5** shares the same origin: it is phosphorescence with a lifetime from tens of microseconds to a few milliseconds. The phosphorescence is a major relaxation channel at low temperatures, referring, for instance, to the quantum efficiency, Φ_{PL}, of ≈ 100 % for **1** and **5** at T = 5 K, as estimated from the PL temperature dependences and Φ_{PL} values measured at room temperature using an integrating sphere (see the supporting information). Furthermore, similar to the alkali metal and calcium complexes, **1–3** and **5** show a TADF-characteristic temperature dependence of the PL decay time, τ, as illustrated in Figure 5 for **5**. Here a strong decrease of τ in the temperature interval from 100 to 200 K reflects a transition from phosphor-

Chemistry–A European Journal

Full Paper
doi.org/10.1002/chem.202101247

Chemistry Europe
European Chemical
Societies Publishing
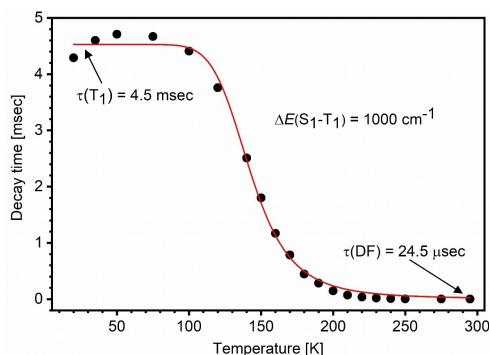
Figure 5. PL decay time of Zn complex **5** versus temperature. PL was excited at 337 nm with a nsec-pulsed laser, recorded at 470 nm and approximated with monoexponential decay curves (Figure S7.9). The red line is a fit to the TADF model of equilibrated states (Eq. (S1) in the supporting information). This estimates the S_1-T_1 energy separation in **5** to be about 1000 cm^{-1}.

Figure 6. Scheme of photophysical processes suggested for copper complexes **2** and **3** (colored arrows: photoexcitation and emission transitions). It is similar to the standard TADF scheme valid for energetically close-lying relaxed excited singlet state S_1 and triplet state T_1, facilitating thermally activated reverse intersystem crossing (rISC) from T_1 to S_1. However, in difference to TADF, S_1 in **2** and **3** efficiently relaxes to the ground state S_0 *nonradiatively* as practically no fluorescence from S_1 is observed (crossed green arrow). It is assumed that the triplet manifold is mainly populated via intersystem crossing from the vertically excited singlet states *$S_{1,n}$.

escence ($\tau = 4.5$ msec) to delayed fluorescence (with an effective decay time of 24 μsec at 295 K). The red curve in Figure 5 represents a fit of the experimental data to the simple TADF model of the thermally equilibrated singlet (S_1) and triplet (T_1) states (for details see the supporting information).[12a,c–e,17] According to this model, the energy separation ΔE between these states is about 1000 cm^{-1} in **5** and 500 cm^{-1} in **1** (Figure S7.10). These values compare well to those determined for the alkali metal and calcium complexes.[11,14] However, delayed fluorescence in **1** and **5** has a relatively low quantum efficiency (9 and 3 %, respectively, at 295 K). The S_1 state in these compounds apparently decays to the ground state mostly nonradiatively. Accordingly, the PL intensity rapidly drops over the phosphorescence-to-TADF crossover temperature interval (Figures 3, 4). Similarly moderate delayed fluorescence efficiencies were found for the related lithium, cesium and calcium compounds.[11,14] Remarkably, this trend towards lower fluorescence quantum efficiency becomes dramatic in the copper complexes **2** and **3**, which emit practically no fluorescence at all. On the other hand, as mentioned above, they show the TADF-characteristic temperature dependence of the PL (phosphorescence) decay time, correlating with a strong, thermally activated decrease of the emission intensity. These parameters vary especially spectacularly in **3**: over the narrow temperature interval of 75–130 K, τ decreases from ca. 280 to 1 μsec (Figure S7.12), while the PL intensity falls by more than 1000-fold (Figure S7.3). By further increasing the temperature above 150 K, the emission vanishes completely. Such photophysical behavior can still be described within the TADF framework, assuming that the excited singlet state S_1 relaxes to the ground state S_0 virtually completely via internal conversion, i.e. nonradiatively (Figure 6). Thermally activated population of S_1 via reversed intersystem crossing (rISC) from the lower but energetically close-lying, triplet state T_1 can thus effectively deplete T_1.

By analogy with TADF, one can designate the last process as "thermally activated phosphorescence quenching". To the best of our knowledge, such behavior has not yet been described in

literature - likely not due to its rarity, but rather due to a still limited number of detailed low-temperature photophysical studies of metal complexes, particularly those without any PL at room temperature. Indeed, it is well established that a small energy gap ΔE(S_1-T_1) generally correlates with a low oscillator strength/ radiative rate (k_{S1r}) of the $S_1 \rightarrow S_0$ fluorescence.[12c] This is mirrored in long S_1 lifetimes defined for efficient TADF emitters, typically up to hundreds of nanoseconds ($k_{S1r} \leq 10^7$ s^{-1}). For instance, the S_1 intrinsic lifetime of 230 nsec was estimated for the sodium iminophosphonamide complex.[11] Apparently, the efficiency of such 'slow' fluorescence critically depends on suppression of the nonradiative decay, i.e. internal conversion $S_1 \rightarrow S_0$ (typical rate $k_{S1n} \approx 10^9$–10^{10} s^{-1} in organic and metallorganic luminophores).[22] This is one of the reasons why the design of efficient TADF emitters is challenging. In this context, the copper complexes **2** and **3** just exemplify the case of a highly dominating nonradiative decay of S_1 ($k_{S1n} \gg k_{S1r}$).

Applying the model of equilibrated S_1 and T_1 states (Eq. S1) to **2** and **3** yields ΔE(S_1-T_1) ≈ 250 and 950 cm^{-1}, respectively (Figures S7.11 and S7.12). However, the assumption of thermal equilibrium between S_1 and T_1 is likely not valid, considering the efficient nonradiative decay of S_1 and a high ratio of ΔE to the thermal energy, kT, at the crossover temperature (≈ 10 for **3**). If the nonradiative decay of S_1 is much faster than the ISC channel $S_1 \rightarrow T_1$, the expression for the temperature-dependent phosphorescence decay time, $\tau(T)$, reduces to (Eq. (1))

$$\tau(T) = \frac{\tau(T_1)}{1 + \tau(T_1)\, A\, \exp\left(-\frac{\Delta E}{kT}\right)} \tag{1}$$

where $\tau(T_1)$ is the intrinsic phosphorescence lifetime and $A \cdot \exp(-\Delta E/kT)$ represents the rate of thermally activated reversed intersystem crossing (rISC) between the T_1 and S_1 states. Note, however, that both Equations (1) and (S1) yield practically the same estimates for the energy separation ΔE, as a result of a

These are not the final page numbers! ↗↗

strong variation of $\tau(T)$ (over three orders of magnitude in **3**), which is described by the exponential factor exp(-$\Delta E/kT$). The experimental estimate of ΔE for the complex **3** was supported by calculations (see below).

In contrast to the compounds discussed above, the PL of **6**, **7** and the major emission of **4** at 500 nm represent prompt fluorescence, also at cryogenic temperatures, with a lifetime < 5 nsec (time resolution of the apparatus used). Such different behavior can be explained by their particular ligand structure and crystal packing. [(R)-NEPIA] ligands of **4** possess phenyl and naphthyl groups. In solid **4**, these groups of neighboring molecules arrange themselves roughly in parallel, at inter- and intramolecular separation distances of 4.1 Å (Figure S6.5). Such arrangement can enable weak π-stacking interactions. In addition to the fluorescence, **4** shows a minor broad emission at 700 nm, which decays within microseconds (Figure 3). Both bands only moderately depend on the temperature. We tentatively ascribe these emissions to, respectively, singlet and triplet excimers or excitons generated in the stacked phenyl-naphthyl units.

The poor triplet formation (absence of phosphorescence / TADF) in **6** might be related to the nearly planar coordination of the NPN backbones of two iminophosphonamide ligands around the zinc atom. In contrast, a strongly bent or twisted geometry is observed in the zinc complex **5** as well as in the dimeric iminophosphonamide complexes of alkali metals and calcium. As mentioned in the introduction, we have attributed the origin of phosphorescence / TADF in the latter compounds to intramolecular charge transfer between the 'monomeric' ligand units, resulting in enhanced intersystem crossing (ISC) and triplet formation.[13] This process is expected to strongly depend on the mutual ligand configuration. For instance, the efficient triplet formation in dimers of BODIPY fluorescent dye molecules - also attributed to intramolecular charge transfer - has only been observed for the orthogonally arranged monomeric units and ceased in their planar configuration.[23] A similar effect may occur in **6**. Somewhat in contradiction to this rationalization, the phosphorescent copper complexes **1–3** also demonstrate a planar arrangement of the two NPN backbones (see above). However, the efficient triplet formation in these complexes can be attributed to the heavy atom effect of the two copper atoms. According to the calculated frontier molecular orbitals of **3** (Figure S9.1), the copper centers are directly involved in the electronic transitions. The highest and lowest molecular orbitals are largely localized on the copper centers and the iminophosphonamide ligands, respectively. Correspondingly, the lowest energy excitation is of mainly metal-to-ligand charge transfer character, similar to many copper(I) d^{10} systems reported in the literature.[15d]

Finally, the zinc complex **7** is the only example among the studied compounds of a single iminophosphonamide ligand coordination. Accordingly, this complex does not match the above scheme suggested for the dimeric iminophosphonamide metal complexes and does not demonstrate efficient triplet formation (a significant effect of zinc on ISC in **7** can be safely ruled out). Instead **7** only shows prompt fluorescence. It is intense at low temperatures, decreases strongly upon increas-

ing the temperature, and likely results from a solely ligand-localized excitation.

Step-scan FTIR spectroscopy and DFT modelling

Time-resolved step-scan FTIR investigations were performed for the copper complex **3** containing the bulky ligands DippPIA⁻ in particular to further characterize its long-lived excited triplet state. **3** was chosen as it shows the most surprising temperature-dependent PL behavior (see above). The samples for transient FTIR experiments were prepared as KBr pellets, a technique which was introduced by Palmer et al.[24] and has been established in the Gerhards group over the last few years.[25] For instance, a series of bi- and tetranuclear OLED (organic light emitting diode) – relevant Cu(I) complexes has recently been investigated with this technique.[25a,c,26]

The measured steady-state (ground state) FTIR spectrum of **3** is in perfect agreement with the IR spectrum calculated within density functional theory (DFT) (Figure 7). Hence, the experimental absorption bands could be assigned to specific vibrations which are listed in the supporting information (Table S8.1). Practically no change in the ground state IR
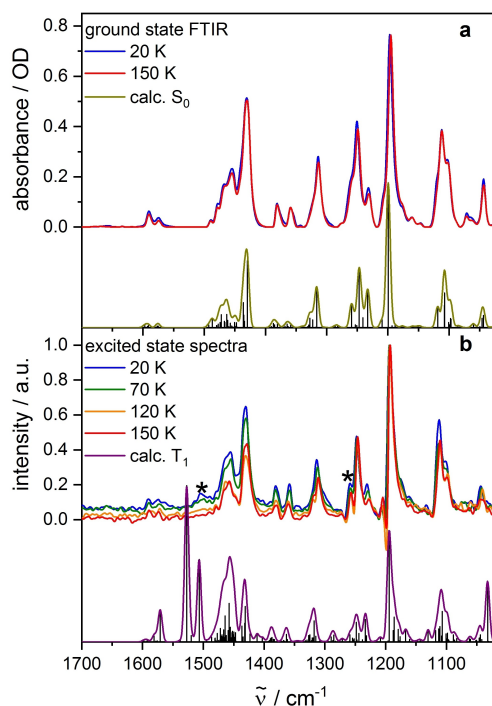
Figure 7. a) Upper trace: FTIR steady-state (ground state, S_0) spectra of **3** at 20 and 150 K. Lower trace: Calculated IR transitions and simulated IR spectrum of the S_0 state. B) Upper trace: experimental excited state IR spectra of **3** at 20, 70, 120 and 150 K obtained from the step-scan difference spectra (averaged over 2 μs after laser pulse). The asterisks indicate distinct bands characteristic for the excited state. Lower trace: Calculated IR transitions and simulated IR spectrum of the T_1 state. Calculations: DFT/B3LYP-D3(BJ)/def2-TZVP, IR absorption frequencies scaled by 0.975, convolution with Gaussian profiles, FWHM = 8 cm⁻¹.

Chemistry–A European Journal

Full Paper
doi.org/10.1002/chem.202101247

Chemistry Europe
European Chemical
Societies Publishing

spectrum was observed between 20 K and room temperature, indicating the persistent crystal structure. The sample was then excited at 20–150 K with 355 nm laser pulses and time-resolved difference IR spectra were recorded. The spectrum shown in Figure S8.1 was averaged over the first 2 µs after the laser pulse (see supporting information for further details).

For a better direct comparison of the measured IR absorption in the electronic ground (S_0) and excited states (Figure 7), the IR absorption spectrum of the latter was generated by addition of 3.5% of the ground state spectrum to the step-scan difference spectrum in order to suppress the negative bands resulting from depopulation of S_0. Interestingly, a new band is observed at 1505 cm^{-1}, where the S_0 state does not absorb, so that this feature is specific for the excited state. Additionally, a distinct peak is observed at 1259 cm^{-1} in the excited state, instead of a shoulder in the S_0 spectrum. The described impact of UV excitation on the IR absorption indicates structural changes. The corresponding excited state can be assigned to the triplet state of **3**.

Indeed, the experimental excited state spectrum is in good agreement with the calculated spectrum of the lowest triplet state T_1 (calculated by unrestricted DFT (UDFT)) with respect to the spectral positions (Figure 7b). The observed specific absorption band slightly above 1500 cm^{-1} most likely corresponds to the prominent doublet of peaks in the calculated spectrum at 1528 and 1507 cm^{-1}. This doublet is an aromatic C-C-stretching vibration in the phenyl substituents on the phosphorous atom of the ligand, whereas the band at 1259 cm^{-1} corresponds to a combined mode involving C-N stretching motion.

Step-scan FTIR investigations were then performed additionally at 70 K, 120 K and 150 K for comparison with the PL data (Figures 7 and S8.2). The corresponding excited state spectra and the underlying step-scan difference spectra are similar to that at 20 K. The absorption around 1505 cm^{-1} diminishes with the temperature, but is recognizable till at least 120 K. Even at 150 K there might be a very weak excited state absorption around 1500 cm^{-1}. This assertion is supported when comparing the step-scan spectra averaged over 0–0.5 µs and 3.0–3.5 µs after laser excitation, where a decay over time is visible to some extent in this spectral region (Figure S8.3). At the same time, the peak at 1259 cm^{-1} is visible in all four spectra. This difference might be due to broadening of the former band at higher temperatures, for example, via coupling to low-energy modes, thus making it difficult to probe spectroscopically. The significant similarities between the excited state spectra at different temperatures are consistent with the same (major) excited state being involved.

Its lifetime was determined from the step-scan data by considering the decay of the most prominent positive and negative bands in the difference IR spectrum over time after laser excitation. These bands were first fitted separately (see, for example, Figure S8.4 for the bleach band at 1199 cm^{-1} at 20 K), yielding input values for a global fit over all chosen bands. A biexponential decay was determined at all probed temperatures (Figures S8.5–8) with strongly temperature-dependent time constants. The time constants of the main component of

about 140 and 83 µs (contribution of 95 and 86%) at 20 and 70 K, respectively, are in reasonable agreement with the PL data (taking into account the different sample preparations and excitation laser intensities in these experiments). On the other hand, the step-scan IR spectroscopy still detects the excited state with an effective lifetime of about 11 µs at 150 K (Table S8.2), whereas the steady-state PL signal is very weak and decays on the sub-microsecond time scale at this temperature (see above). This discrepancy might indicate that the photophysical scheme in Figure 6 – primarily focused on the emissive excited states - is oversimplified for **3** and some other non-emissive long-lived (triplet) state might be involved. It may be minor below 100 K, but dominant over microseconds after laser pulse excitation at higher temperatures. This issue requires further investigation. In addition to the frontier molecular orbitals (Figure S9.1), we illustrate the electronic character of the T_1 state of **3** by a spin density plot (Figure 8).

It clearly indicates spin localization on the phenyl groups, nitrogen atoms and, to a minor extent, on the copper atoms. This correlates with the structural changes in the excited state: for instance, asymmetric NPN bite angles of 98.4° and 108.1° were calculated for the two iminophosphonamide units of **3** in the T_1 state, compared to the equal angles of 108.5° in the S_0 state. The structural parameters of the S_0 and T_1 states are listed in the supporting information (Table S9.1).

Conclusions

We described the synthesis of a series of binuclear Cu(I) and mononuclear Zn(II) iminophosphonamide complexes. Four differently substituted iminophosphonamide ligands were employed. Except the Zn complex **7** with a single iminophosphonamide ligand, they all adopt coordination of two ligands to the metal centers, similar to the structurally related alkali metal and calcium complexes.[11,14] Due to the different steric demand of the substituents the arrangement of the complexes in the solid-state varies slightly, which influences the photophysical proper-
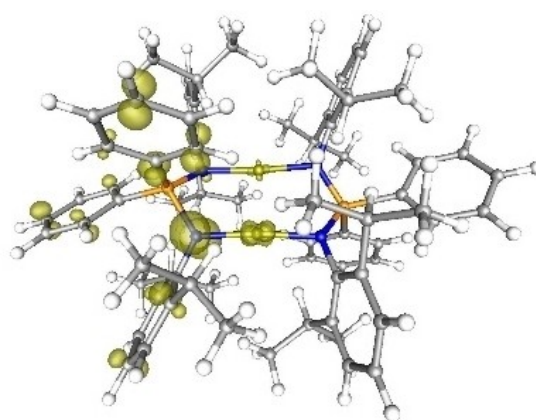
Figure 8. Spin density of **3** in its T_1 state (isovalue: 0.01 a.u.) (DFT/B3LYP-D3(BJ)/def2-TZVP). It localizes mainly at the phenyl rings and the N atoms of the iminophosphonamide ligand.

Chemistry–A European Journal | Full Paper
doi.org/10.1002/chem.202101247

Chemistry
Europe
European Chemical
Societies Publishing

ties. Some of the Cu(I) and Zn(II) complexes show bright long-lived phosphorescence in the solid state at low temperatures (< 100 K), which transforms into thermally activated delayed fluorescence (TADF) at elevated temperatures - similar to their alkali metal and calcium analogues. While the PL of two Cu complexes (**2**, **3**) can also be described within the TADF scheme, there is a qualitative difference insofar as these complexes, involve the *non-emissive* relaxed singlet excited state S_1 coupled by intersystem crossing (ISC) to the low-lying *emissive* triplet state T_1. Accordingly, **2** and **3** show bright phosphorescence below ≈ 80 K, its thermally activated quenching in the narrow temperature interval above ≈ 80 K, and practically no PL above ≈ 150 K. Transient step-scan FTIR spectroscopy on the Cu complex **3** allowed further probing of the T_1 state. The step-scan FTIR spectra revealed a characteristic T_1 state vibration assigned to the phenyl stretching mode on the basis of DFT calculations. This mode in turn fingerprints the structural relaxation of **3** upon population of the T_1 state. In contrast, two Zn complexes (**6**, **7**) were found to exhibit solely prompt fluorescence. The poor triplet formation in these compounds was attributed to their particular ligand coordination. The present work thus further illustrates the very diverse PL properties of metal complexes based on iminophosphonamide ligands.

Remarkably, the energy levels of the S_1 and T_1 states appear rather similar (and energetically close to each other) in most of iminophosphonamide metal complexes studied so far.[11,14] In this regard, the specific ligand structure and coordination arrangement primarily affect the rates of transitions within a common framework of ground and excited states. Of particular interest is the possibility to strongly influence ISC efficiency and corresponding triplet formation (as well as TADF output) via subtle changes in ligand design and choice of the metal centers/ coordination.

From application point of view, the iminophosphonamide metal complexes studied so far cannot compete in terms of quantum efficiency and, very importantly, processing with well-established TADF emitters like purely organic 2,4,5,6-tetra(9H-carbazol-9-yl)isophthalonitrile.[12b] However, we believe that both synthetic and photophysical potential of this class of luminescent metal complexes is by far not fully explored and may promise further examples with interesting (and perhaps also practically relevant) photophysical properties.

Experimental Section

Experimental details are given in the supporting information. The supporting information also compiles crystallographic and spectroscopic data for all new compounds (^{1}H, ^{13}C{^{1}H}, ^{31}P{^{1}H} NMR, IR, Raman and PL spectra), as well as additional data from step-scan FTIR experiments and DFT calculations.

Deposition numbers 2075954 (**1**), 2075955 (**2**), 2075956 (**3**), 2075957 (**4**), 2075958 (**5**), 2075959 (**6**), and 2075960 (**7**) contain the supplementary crystallographic data for this paper. These data are provided free of charge by the joint Cambridge Crystallographic Data Centre and Fachinformationszentrum Karlsruhe Access Structures service.

[1] A. Steiner, S. Zacchini, P. I. Richards, *Coord. Chem. Rev.* **2002**, *227*, 193–216.
[2] F. T. Edelmann, *Chem. Soc. Rev.* **2012**, *41*, 7657–7672.
[3] A. M. Kalsin, T. A. Peganova, I. S. Sinopalnikova, I. V. Fedyanin, N. V. Belkova, E. Deydier, R. Poli, *Dalton Trans.* **2020**, *49*, 1473–1484.
[4] S. Takahashi, J. Sekiguchi, A. Ishii, N. Nakata, *Angew. Chem. Int. Ed.* **2021**, *60*, 4055–4059; *Angew. Chem.* **2021**, *8*, 4101–4105.
[5] a) C. Fedorchuk, M. Copsey, T. Chivers, *Coord. Chem. Rev.* **2007**, *251*, 897–924; b) D.-Y. Lu, T.-S. Kuo, Y.-C. Tsai, *Angew. Chem. Int. Ed.* **2016**, *55*, 11614–11618; *Angew. Chem.* **2016**, *38*, 11786–11790.
[6] a) S.-O. Hauber, F. Lissner, G. B. Deacon, M. Niemeyer, *Angew. Chem. Int. Ed.* **2005**, *44*, 5871–5875; *Angew. Chem.* **2005**, *36*, 6021–6025; b) C. GuhaRoy, R. J. Butcher, S. Bhattacharya, *J. Organomet. Chem.* **2008**, *693*, 3923–3931; c) M. R. Gyton, A. R. Leverett, M. L. Cole, A. I. McKay, *Dalton Trans.* **2020**, *49*, 5653–5661.
[7] a) F. Pauer, J. Rocha, D. Stalke, *J. Chem. Soc. Chem. Commun.* **1991**, 1477–1479; b) R. Fleischer, B. Walfort, A. Gbureck, P. Scholz, W. Kiefer, D. Stalke, *Chem. Eur. J.* **1998**, *4*, 2266–2274; c) M. M. Meinholz, S. K. Pandey, S. M. Deuerlein, D. Stalke, *Dalton Trans.* **2011**, *40*, 1662–1671.
[8] B. Prashanth, S. Singh, *J. Chem. Sci.* **2015**, *127*, 315–325.
[9] A. Stasch, *Chem. Eur. J.* **2012**, *18*, 15105–15112.
[10] a) S. Bestgen, C. Schoo, B. L. Neumeier, T. J. Feuerstein, C. Zovko, R. Köppe, C. Feldmann, P. W. Roesky, *Angew. Chem. Int. Ed.* **2018**, *57*, 14265–14269; *Angew. Chem.* **2018**, *43*, 14461–14465; b) M. K. Rong, F. Holtrop, J. C. Slootweg, K. Lammertsma, *Coord. Chem. Rev.* **2019**, *382*, 57–68; c) C. Zovko, S. Bestgen, C. Schoo, A. Görner, J. M. Goicoechea, P. W. Roesky, *Chem. Eur. J.* **2020**, *26*, 13191–13202.
[11] T. J. Feuerstein, B. Goswami, P. Rauthe, R. Köppe, S. Lebedkin, M. M. Kappes, P. W. Roesky, *Chem. Sci.* **2019**, *10*, 4742–4749.
[12] a) A. Endo, M. Ogasawara, A. Takahashi, D. Yokoyama, Y. Kato, C. Adachi, *Adv. Mater.* **2009**, *21*, 4802–4806; b) H. Uoyama, K. Goushi, K. Shizu, H. Nomura, C. Adachi, *Nature* **2012**, *492*, 234–238; c) Y. Tao, K. Yuan, T. Chen, P. Xu, H. Li, R. Chen, C. Zheng, L. Zhang, W. Huang, *Adv. Mater.* **2014**, *26*, 7931–7958; d) H. Yersin, R. Czerwieniec, M. Z. Shafikov, A. F. Suleymanova, *Highly Efficient OLEDs: Materials Based on Thermally Activated Delayed Fluorescence*, Wiley Periodicals, Weinheim, **2018**, p. 1; e) T. J. Penfold, F. B. Dias, A. P. Monkman, *Chem. Commun.* **2018**, *54*, 3926–3935.
[13] H. Khandelwal, A. R. Mallia, R. T. Cheriya, M. Hariharan, *Phys. Chem. Chem. Phys.* **2012**, *14*, 15282–15285.
[14] B. Goswami, T. J. Feuerstein, R. Yadav, R. Köppe, S. Lebedkin, M. M. Kappes, P. W. Roesky, *Chem. Eur. J.* **2021**, *27*, 4401–4411.
[15] a) D. M. Zink, M. Bächle, T. Baumann, M. Nieger, M. Kühn, C. Wang, W. Klopper, U. Monkowius, T. Hofbeck, H. Yersin, S. Bräse, *Inorg. Chem.* **2013**, *52*, 2292–2305; b) D. M. Zink, T. Baumann, J. Friedrichs, M. Nieger, S. Bräse, *Inorg. Chem.* **2013**, *52*, 13509–13520; c) M. J. Leitl, V. A. Krylova, P. I. Djurovich, M. E. Thompson, H. Yersin, *J. Am. Chem. Soc.* **2014**, *136*, 16032–16038; d) R. Czerwieniec, M. J. Leitl, H. H. H. Homeier, H. Yersin, *Coord. Chem. Rev.* **2016**, *325*, 2–28; e) M. Klein, N. Demirel, A. Schinabeck, H. Yersin, J. Sundermeyer, *Molecules* **2020**, *25*, 3990; f) G. U. Mahoro, J. Fernandez-Cestau, J.-L. Renaud, P. B. Coto, R. D. Costa, S. Gaillard, *Adv. Opt. Mater.* **2020**, *8*, 2000260.

[16] a) H. Ackermann, O. Bock, U. Müller, K. Dehnicke, *Z. Anorg. Allg. Chem.* **2000**, *626*, 1854–1856; b) T. J. Feuerstein, *Synthese photolumineszenter Metallkomplexe, UV-LED NMR-Charakterisierung eines photolabilen Komplexes sowie photolithographische Immobilisierung von Metallopolymeren*, PhD Thesis, Karlsruhe Institute of Technology (KIT), Kalrsruhe, Germany, **2019**; c) B. Goswami, *Enantiopure Iminophosphonamide Complexes: Synthesis, Photoluminescence and Catalysis*, PhD Thesis, Karlsruhe Institute of Technology (KIT), Kalrsruhe, Germany, **2020**.

[17] M. J. Leitl, F.-R. Küchle, H. A. Mayer, L. Wesemann, H. Yersin, *J. Phys. Chem. A* **2013**, *117*, 11823–11836.

[18] A. C. Lane, C. L. Barnes, W. E. Antholine, D. Wang, A. T. Fiedler, J. R. Walensky, *Inorg. Chem.* **2015**, *54*, 8509–8517.

[19] B. S. Lim, A. Rahtu, J.-S. Park, R. G. Gordon, *Inorg. Chem.* **2003**, *42*, 7951–7958.

[20] Z. Chen, A. Lohr, C. R. Saha-Möller, F. Würthner, *Chem. Soc. Rev.* **2009**, *38*, 564–584.

[21] M. Llunell, P. Alemany, S. Alvarez, Shape 2.1 for Windows (32 bit). Available from: http://www.ee.ub.edu/index.php?option=com_jdown-loads&view=viewcategories&Itemid=529. Accessed: 09/03/2021.

[22] J. R. Lakowicz, *Principles of Fluorescence Spectroscopy* (Ed.: J. R. Lako-wicz), Springer US, Boston, MA, **2006**, p. 1.

[23] a) Y. Cakmak, S. Kolemen, S. Duman, Y. Dede, Y. Dolen, B. Kilic, Z. Kostereli, L. T. Yildirim, A. L. Dogan, D. Guc, E. U. Akkaya, *Angew. Chem.*

Int. Ed. **2011**, *50*, 11937–11941; *Angew. Chem.* **2011**, *50*, 12143–12147; b) N. Epelde-Elezcano, E. Palao, H. Manzano, A. Prieto-Castañeda, A. R. Agarrabeitia, A. Tabero, A. Villanueva, S. de la Moya, Í. López-Arbeloa, V. Martínez-Martínez, M. J. Ortiz, *Chem. Eur. J.* **2017**, *23*, 4837–4848.

[24] G. D. Smith, M. S. Hutson, Y. Lu, M. T. Tierney, M. W. Grinstaff, R. A. Palmer, *Appl. Spectrosc.* **2001**, *55*, 637–642.

[25] a) M. Zimmer, F. Dietrich, D. Volz, S. Bräse, M. Gerhards, *ChemPhysChem* **2017**, *18*, 3023–3029; b) M. Dorn, J. Kalmbach, P. Boden, A. Päpcke, S. Gómez, C. Förster, F. Kuczelinis, L. M. Carrella, L. A. Büldt, N. H. Bings, E. Rentschler, S. Lochbrunner, L. González, M. Gerhards, M. Seitz, K. Heinze, *J. Am. Chem. Soc.* **2020**, *142*, 7947–7955; c) P. Boden, P. Di Martino-Fumo, J. M. Busch, F. R. Rehak, S. Steiger, O. Fuhr, M. Nieger, D. Volz, W. Klopper, S. Bräse, M. Gerhards, *Chem. Eur. J.* **2021**, *27*, 5439–5452.

[26] J. M. Busch, D. M. Zink, P. Di Martino-Fumo, F. R. Rehak, P. Boden, S. Steiger, O. Fuhr, M. Nieger, W. Klopper, M. Gerhards, S. Bräse, *Dalton Trans.* **2019**, *48*, 15687–15698.

FULL PAPER

To glow or not to glow: Chiral imino-phosphonamide copper and zinc complexes are presented. Some steady-state and time-resolved photoluminescence (PL) features studied at low temperatures can be described within the thermally activated delayed fluorescence (TADF) scheme. However, unusually, the fluorescence is nearly absent in two complexes and the low-lying triplet state quenches PL. Some excited states were further investigated by time-resolved FTIR spectroscopy and quantum chemical calculations.
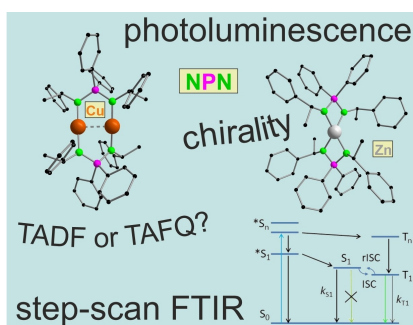
Dr. B. Goswami, Dr. T. J. Feuerstein, Dr. R. Yadav, Dr. S. Lebedkin, P. J. Boden, S. T. Steiger, Prof. Dr. G. Niedner-Schatteburg, Prof. Dr. M. Gerhards, Prof. Dr. M. M. Kappes, Prof. Dr. P. W. Roesky*

1 – 11

Thermally Activated Delayed Fluorescence and Phosphorescence Quenching in Iminophosphonamide Copper and Zinc Complexes